Biomechanical analysis of time-developing interconnected tree systems

Wang, Xiuli; Gard, Wolfgang; Kamath, Abhijith; van de Kuilen, Jan Willem

DOI
10.1016/j.tfp.2025.101023

Publication date
2025

Document Version
Final published version

Published in
Trees, Forests and People

Trees, Forests and People 22 (2025) 101023

Contents lists available at ScienceDirect

Trees, Forests and People

journal homepage: www.sciencedirect.com/journal/trees-forests-and-people

Biomechanical analysis of time-developing interconnected tree systems

Xiuli Wang [a,b,*], Wolfgang Gard [a], Abhijith Kamath [a], Jan-Willem van de Kuilen [a,c]

[a] Biobased Structures and Materials, Faculty of Civil Engineering and Geosciences, Delft University of Technology, Delft, The Netherlands
[b] Institute of Bio- and Geosciences, IBG-2: Plant Sciences, Forschungszentrum Jülich GmbH, Jülich, Germany
[c] Wood Technology, Department of Materials Engineering, Technical University of Munich, Munich, Germany

ARTICLE INFO

Keywords:
Adaptive growth
Pulling test
Inosculation
Interconnected trees
Tree stability

ABSTRACT

Enhancing urban tree stability is critical for public safety and infrastructure protection. This study evaluates a nature-based method for improving tree stability using inosculations to form interconnected tree systems. These systems establish biomechanical connections through inosculation, offering both biological and mechanical support. The research focused on lime trees (*Tilia Cordata* Mill.), comparing parallel and cross connected tree systems with the single tree to evaluate their mechanical performance. The mechanical performance of the interconnected tree systems was evaluated by pulling tests in different directions to simulate wind loads. The study spanned a two-year growth period to investigate the effects of growth on mechanical behavior, with the analysis supported by finite element modeling. The results showed that growth-induced changes increased the overall rigidity of the tree systems and reduced deformation, rotation, and local elongation. Cross connected trees exhibited notable bracing effects in the connected plane, which improved lateral resistance. In a parallel connected tree system, the basal stiffness increased due to the connection between the lower region. Compared to the single tree, interconnecting tree systems can provide additional support and reduce deformation caused by lateral loads, making it a promising strategy to improve tree stability under horizontal loads.

1. Introduction

Wind is a key abiotic factor shaping urban tree dynamics. Its impact extends beyond mechanical damage to trees, as it also serves as an essential environmental signal for tree growth (Gardiner and Quine, 2000; Alméras and Fournier, 2009; Moulia et al., 2015; Gardiner et al., 2016). While excessive wind loads pose risks of tree failure, wind-induced mechanical stress also triggers the adaptive growth of trees (i.e., thigmomorphogenesis) (Telewski, 2012; Hamant and Moulia, 2016; Dlouhá et al., 2025). A natural phenomenon of tree adaptive growth is the fusion of trees with boundary obstacles or neighboring trees. This process helps trees gain structural support or attachment. For example, as shown in Fig. 1a, the tree can integrate with steel supports for the enhancement of its stability. In forest ecosystems, the root grafting (Fig. 1b) is a more common fusion phenomenon. Trees connect through their root systems, through which trees gain resources exchange and also improve root anchorage to some extent (Tarroux et al., 2010; Vovides et al., 2021; Kragler and Bock, 2025). Beyond root grafting, stem fusion is another frequent phenomenon in forests (Goldschmidt, 2014; Melnyk, 2017). Stems of the same tree species, such as willows (Ludwig et al., 2012; Middleton et al., 2023), weeping figs (Wang et al., 2025a), and small-leaved limes (Wang et al., 2020) can fuse together. This process forms an interconnected tree system that maintains both structural integrity and growing activity (Wang et al. 2025b). The example of weeping figs is shown in Fig. 1c; and it has a braided net formed by six individual tree stems. The individual structural component in this net is an inosculated connection (i.e., self-growing connection in (Wang et al., 2020, 2025b)).

Previous studies on self-growing connections (Wang et al., 2025a, b) found that the bond between two trees occurs through the integration of the vascular cambium layer, which provides the starting point of the formation of a connection. This enables the growth of new wood tissues at the fusion interface. As illustrated in Fig. 1d, the dashed marker shows the fiber bundles that connect two stems. Additional cross sections of the connection (Fig. 1e and f) also show continuous fiber bundles that bond the stems. The spatial distribution and orientation of these fibers result from anisotropic optimization of trees on multi-scales. At the cellular level, trees produce reaction wood (Fig. 1*g*) in response to mechanical stimuli. This specialized wood formation further enhances structural strength in the intersected region and ensures the integrity of the

* Corresponding author.
E-mail addresses: xiu.wang@fz-juelich.de (X. Wang), W.F.Gard@tudelft.nl (W. Gard), A.C.Kamath@tudelft.nl (A. Kamath), vandekuilen@hfm.tum.de (J.-W. van de Kuilen).

https://doi.org/10.1016/j.tfp.2025.101023

Available online 22 September 2025

interconnected tree system.

From the perspective of structural engineering, the bonding formation of a connection by two trees results in an interconnected structural system (Lievestro, 2020; Wang et al., 2020). In this system, individual trees act as structural components, while the self-growing connection serves as the joint point. This natural and connecting system is able to achieve both structural integrity and growth adaptability. Research on this system is still at an exploratory stage, with simplified preliminary pulling tests having been conducted (Wang et al., 2020; Middleton et al. 2023). Still, it remains unclear how the biological characteristics of the interconnected trees evolve during growth and how these changes affect their mechanical performance. Therefore, in this study, interconnected tree systems (Fig. 2a) using cross (Fig. 2b) and parallel connections (Fig. 2c) are cultivated, with the aim to compare the lateral resistance between single trees and interconnected trees over the course of growth. It is hypothesized that due to the existence of the connection in the interconnected tree system, the system can jointly resist lateral loads and redistribute loads among individual trees, resulting in a higher lateral resistance than that of a single tree.

The wind resistance of a tree refers to its ability to withstand strong winds without internal wood damage, stem breakage, or uprooting, which can lead to structural failure (Gardiner and Quine 2000; Cucchi et al., 2005; Peltola, 2006). On larger scales (such as forest stands or regions), wind resistance is influenced by multiple factors including climate conditions, stand structure, terrain exposure, soil properties, and soil preparation (Dupuy et al., 2005; Sellier and Fourcaud, 2009). Other biotic and abiotic stressors, such as drought, stem decay, and root rot, also play a role (Nicoll et al. 2006; Dlouhá et al. 2024). At the individual tree level, the resistance to wind is affected by phenotypic characteristics, structural characteristics, wood strength, and density (Gardiner and Quine 2000; Peltola 2006). The variability among these factors further complicates the analysis of wind resistance. For uprooting, the primary resistance depends on root anchorage, which is determined by the critical overturning moment (Stokes et al., 2005; Fourcaud et al., 2008). Root anchorage is considered a function of stem volume (Dupuy et al., 2005; Lundström et al., 2007b). On the other hand, the resistance to breakage of the stem depends mainly on the strength of the wood and the diameter of the stem (Cucchi et al., 2005; Peltola, 2006). The analysis of wind resistance of interconnected trees is based on the knowledge of individual trees and on the geometry of the interconnected trees.

In experimental studies of tree wind resistance, the static tree pulling test is commonly used (Cucchi et al., 2005; Peltola, 2006; Dahle et al., 2017; Detter et al., 2023; Middleton et al., 2023). This method provides detailed information on the mechanical response of a tree to wind and is considered a practical approach to quantifying the mechanical stability of trees. For more detailed analysis, researchers have adopted the finite element method (FEM), particularly to model tree architecture (Sellier et al., 2006; Jackson et al., 2019a). This approach reduces experimental costs while improving the accuracy of wind resistance predictions.

Building on existing research on wind resistance of a single tree, this study investigates three types of tree systems: single tree, parallel interconnected trees, and cross interconnected trees. A non-destructive in situ pulling test was performed before and after a two-year growth period. Multiple loading scenarios were tested on interconnected tree systems. This allowed for comparison of changes in lateral resistance at different stages of growth. In parallel, FEM was used to evaluate the mechanical behavior and structural stability of the three systems, providing a comprehensive assessment of their performance against wind.

2. Materials and methods

2.1. Layout of interconnected tree systems

The three tree systems studied in this investigation, including single tree (TS), parallel connected trees (TPA and TPB, as in Fig. 2c), and cross connected trees (TCA and TCB, as in Fig. 2b), are located in the Hortus Botanicus of TU Delft, the Netherlands (latitude: 52°00′3.60″ N, longitude: 4°22′12.5″E). The name of a sample indicate its connecting configuration; for example, TCA refers to the cross connected one, while TPA denotes a parallel connected tree. The parallel connection is located in the lower part of TPA and TPB at approximately 0.5 m above ground. The cross connection was formed by TCA and TCB and located at a height of 2.2 m, above the location of the first branch in the tree TCB. All trees are small-leaved lime (*Tilia Cordata* Mill.), and were planted in November 2010 (Nuijten, 2011). The connections were formed by compressing the bark interfaces of adjacent stems and bounding them

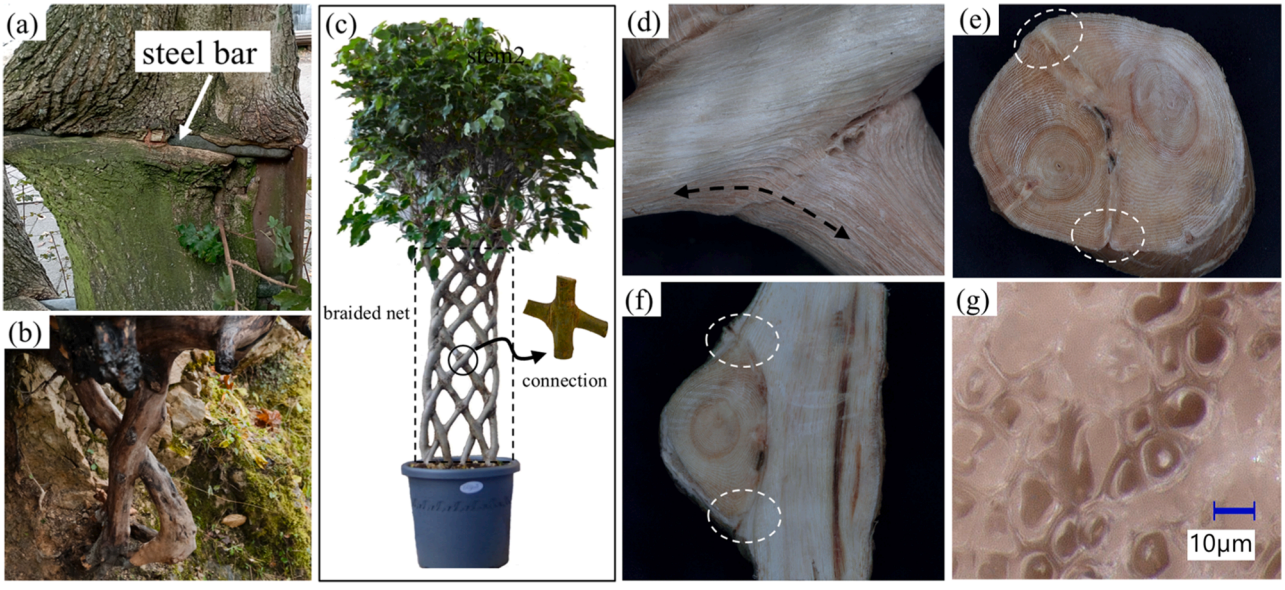

Fig. 1. Adaptive growth features of trees through fusion and structural support. (a) Stem merging with a steel scaffold through integrated growth; (b) A root grafting example; (c) Braided net structure formed by the fusion of six fig tree stems, with each intersection functioning as a self-growing connection; (d) Merged fibers formed at the intersected area, indicated by dashed lines; (e) Transverse section and (f) longitudinal section showing the location of the merged fibers, highlighted with dashed circles; (g) Reaction wood in the fused region (Wang et al. 2025a, b).

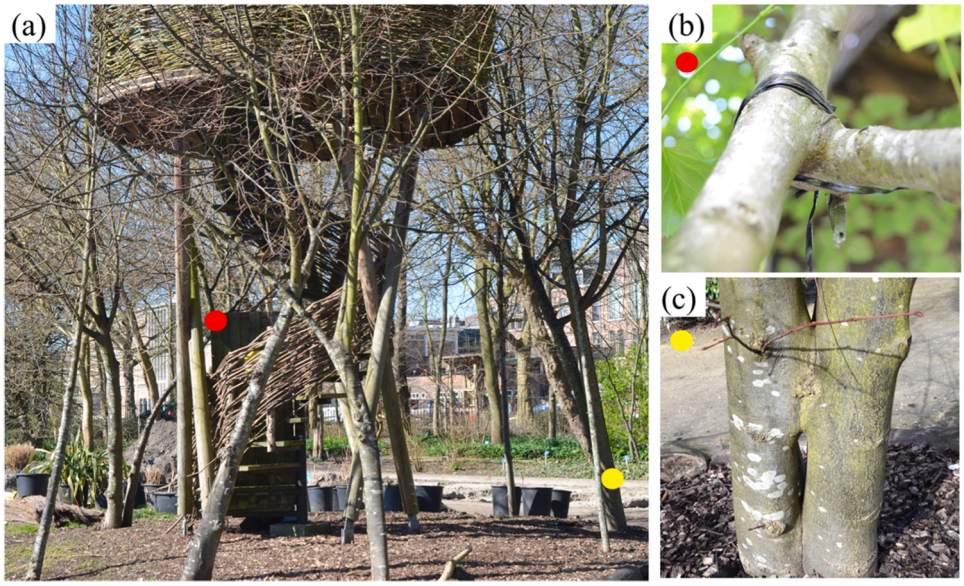

Fig. 2. Interconnected tree systems. (a) Site layout; (b) Cross connected tree system; (c) Parallel connected tree system.

with elastic ropes. Ropes were removed after two growing seasons, by which time the connections had fully merged. All trees were five years old at the time of planting, with similar stem diameters. The spatial arrangement of the three systems is illustrated in Fig. 3. TS, TCA-TCB, and TPA-TPB were distributed around a central point O in the horizontal planting layout. This central point also served as a reference for subsequent measurements and modeling.

2.2. Measurement on the geometry of trees

Geometric changes were measured on all studied trees. Different from the single tree, due to the presence of a connection, the interconnected tree system contains a plane forming by tree components and their bonding connection. For example, in terms of the cross connected trees (Fig. 4), the tree components form a closed triangle configuration by the connection and result in different mechanical performance. Thus, mechanical loading and performance involves both in-plane and out-of-plane cases. The loading and responses that occur within plane *zy* are referred to as in-plane performance. In contrast, those perpendicular to it are defined as out-of-plane (Fig. 4).

To capture the geometric characteristics of the trees, both the variation in cross-sectional size and the potential inclination of growth were considered (see Fig. 4a and b). Using the central point O as the reference point, internal points along the stem were marked at 10 cm intervals in the vertical direction. At each marked point, the diameters along two orthogonal directions on the cross-section were measured. The position of each marked point was determined by projecting it vertically onto the ground and recording its location in the ground coordinate system. As illustrated in Fig. 4b, the spatial position of each internal point was defined in a Cartesian coordinate system. Combined with diameter measurements, the geometry of the tree could be reconstructed. The first measurement was conducted on June 12, 2020, and was referred to as stage I in this study. The second measurement was carried out on June 10, 2022, referred to as stage II. Only the main stem was measured, avoiding knots or branch junctions, up to a height of 3 m. The measurement precision was within 1 mm.

Table 1 summarizes the geometric changes of the three tree systems before and after two years of growth (stage I and stage II). The diameter at breast height (DBH) was measured 1.5 m above the ground. The slenderness ratio was calculated as the ratio of tree height to DBH. The

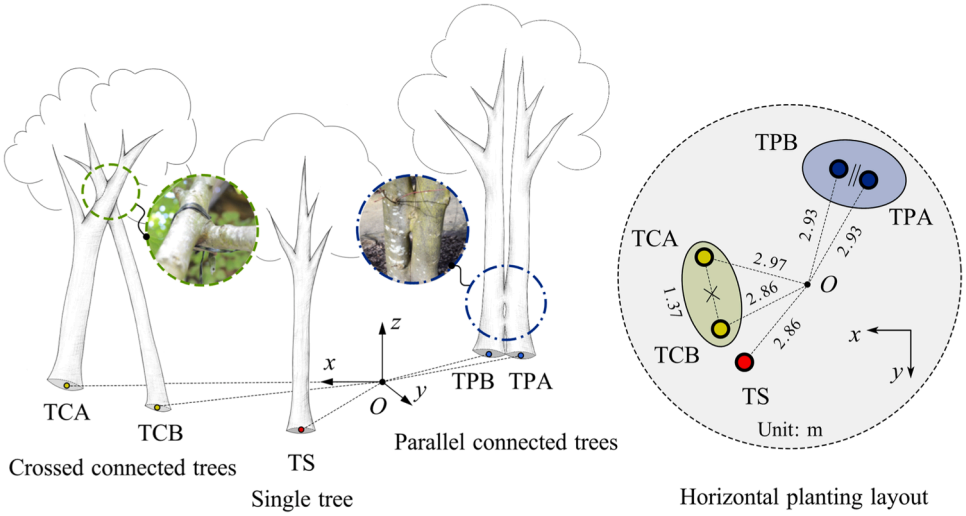

Fig. 3. Illustration of the spatial arrangement of the experimental trees.

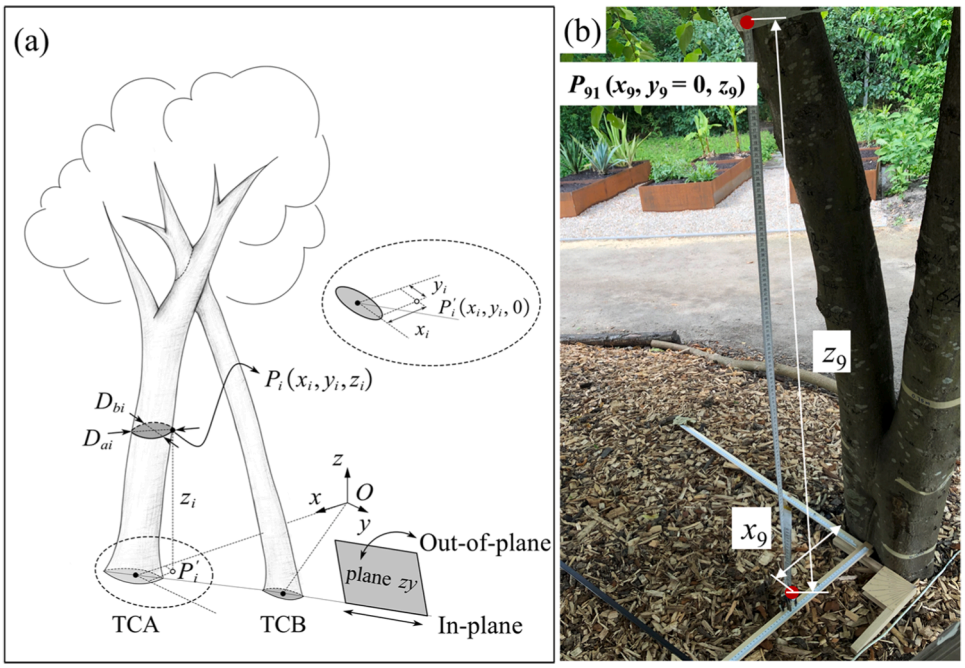

Fig. 4. Example of geometric measurement of tree stems. (a) Using a cross connected tree system (TCA and TCB) as an example, the in-plane loading and response are defined within the intersection plane, while the out-of-plane direction refers to the perpendicular axis. From the center point O, measurement points P_i are placed every 10 cm along the inner curve of the stem. At each point, the spatial position is recorded, and two orthogonal diameters (D_{ai} and D_{bi}) are measured; (b) Field measurement example showing the location and method used to determine point P_{91}.

Table 1
Geometric information of single and connected trees.

Tree ID	Height (m)		DBH (cm)		Slenderness		Stem volume (cm^3)	
	Stage I	Stage II	Stage I	Stage II	Stage I	Stage II	Stage I	Stage II
TS	6.2	8	10.6	14	58.5	57.1	28,600	48,500
TCA	6	7.5	10	12.6	60	59.5	18,400	30,100
TCB	5.5	7	4.9	6.7	112.2	104.5	7500	12,200
TPA	7.3	8	11.9	14.2	61.3	56.3	25,500	39,000
TPB	7.3	8	10	12.4	73	64.5	18,700	29,100

Note: DBH refers to diameter at the breast height; Slenderness = Height/DBH; Stage I indicates the measurement before the two-year growth, and stage II denotes the measurement after.

stem volume was uniformly compared based on measurements taken within the 3 m height range. In this study, the single tree TS tree serves as the primary reference. Within the cross connected tree system, TCA has a size comparable to TS. Similarly, trees TPA and TPB in the parallel connected system also exhibit dimensions close to that of TS.

The mechanical changes caused by cross-sectional growth in the tree are mainly evaluated by comparing the moment of inertia at two different growth stages. Since the moment of inertia is proportional to the bending resistance, it reflects the improvement in structural performance. The moment of inertia is calculated based on Eq. (1).

$$I_{\text{Tree ID}}(H) = \frac{\pi}{64} D^4(H), \tag{1}$$

where I represents the moment of inertia, with units of cm^4; Tree ID refers to single tree (TS), crossed tree systems (TCA and TCB), and parallel tree systems (TPA and TPB); H is the measurement height in cm; and D is the average of the diameters measured on both sides at that height, also in cm.

2.3. Pulling tests setup and procedures

Pulling tests were conducted in stage I and repeated under the same conditions in stage II to ensure comparability of the data across the two-year growth period. The experimental setup was similar to those described in previous studies (Detter et al. 2023; Middleton et al. 2023). As illustrated in Fig. 5a, using the in-plane pulling test of the cross connected tree system as an example, the pulling force was applied through a cable pulling system. The force was measured using a load cell mounted on the cable, with a resolution of 0.01 kN. The angle between the rope and the horizontal plane was recorded using a digital angle sensor integrated into the load cell. The direction of the applied force forms two angles with reference planes. The angle between the force direction and the vertical axis is denoted as α. The angle between the force direction and the cross plane defined by TCA and TCB is denoted β. Together, these two angles define the orientation of the tensile force in a three-dimensional space. The pulling speed was controlled within the range of 50 to 80 mm/min.

During the loading process, the elastometer and inclinometer (PiCUS TreeQinetic testing system, Germany) were installed to measure the local deformation of the wood and root rotations (Fig. 5b). The elastometers measured deformation of the outer xylem fibers by tracking the relative displacement between two pins placed 200 mm apart. Each pin was inserted 20 mm below the bark surface. To capture the rotational movement of the tree during tensile loading, the inclinometer was installed at the base of the tree to monitor angular changes. The resolution of the elastometer was 0.1 μm, and the inclinometer had a

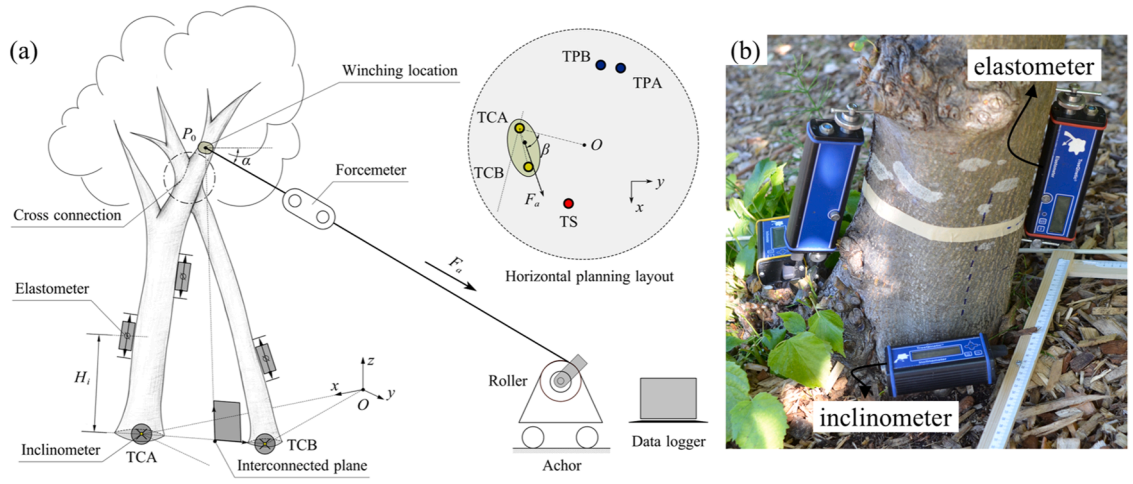

Fig. 5. Setup and schematic illustration of the in-plane pulling test for cross connected tree system. (a) Experimental setup and measurement positions H_i, with the loading direction defined by two spatial angles α and β; (b) The arrangement of the elastometer and inclinometer.

resolution of 0.002°.

In each pulling test, the strain was measured at three to four positions along the stem. At each position, three repeated measurements were taken. According to the findings of (Wessolly and Erb 2016), the region between one-third and two-thirds of the height of the stem is the most susceptible to failure. Therefore, a measurement was placed within this height range for the prediction of failure. To account for structural differences among the three tree systems, five loading scenarios were designed for the tensile tests. These scenarios are illustrated in Fig. 6 and summarized in Table 2. The measurement height and loading height in Table 2 correspond to the illustrated symbols in Fig. 6. Furthermore, abbreviations were introduced to simplify the representation of loading cases: MIP denotes measurements under in-plane loading conditions, while MOP refers to measurements on out-of-plane loading. For the cross connected configuration, the loading point was further distinguished: loads applied above the connection were denoted as MOPU, whereas loads applied directly at the connection were denoted as MOPA.

The first loading case (M-TS) was conducted on the single tree TS (Fig. 6a). It serves as a reference case for the comparison with cross connected trees and is also used to validate the finite element model. The second case (MIP-TPA-B) involved in-plane pulling loading of the parallel connected tree system (Fig. 6b). This configuration represents a structurally vulnerable condition for the interface connection, where splitting is likely to occur. Therefore, it is considered the representative scenario for this system. The third case (MIPU-TCA-B) corresponds to the in-plane pulling loading of the cross connected tree system (Fig. 6c). The fourth (MOPA-TCA-B) and fifth (MOPU-TCA-B) cases both involve out-of-plane loading of the cross connected system (Fig. 6d). The key difference is that in the fourth scenario, the load is applied directly to the connection, allowing a comparison with the third scenario to assess how the loading subjected to the connection influences the structural response.

All in situ pulling tests were conducted within the elastic range of the trees to prevent damage to the stems and connections. To ensure this, the local strain was limited to within 300 μm (approximately ± 0.15 % strain), and the angular deformation was restricted to within 0.05°. The test was terminated immediately once either of these elastic thresholds was reached. The meteorological conditions during the tests were recorded, with a daily mean wind speed 3.3 m/s, the mean temperature 24.3 °C, and no precipitation during the tests. To assess soil moisture conditions, soil samples were taken approximately 15 cm below the surface along the midpoint of the line that connects each tree to the central point O. The moisture content was determined by comparing the fresh and dry weights of the samples, with drying carried out at 105 °C to reach a constant weight. In both test stages, the soil moisture content remained within the range of 20 % to 30 %.

During the test, the directly recorded data included the applied pulling forces, the local deformation measured by elastometers, and the basal rotation measured by inclinometers. A linear regression was performed between the applied forces and both deformation and rotation. Only datasets with a coefficient of determination $R^2 > 0.95$ were considered valid for analysis. To compare the changes in deformation and rotation before and after two years of growth, these fitting results were used. For the comparison of local deformation, the strains at the measurement point as in Eq. (2).

$$\in_i = \frac{\Delta l_i}{200} \times 100\%, \tag{2}$$

where, $\in_i$ represents the strain at measurement point i in two stages. The strain is calculated as the ratio between the deformation of the elastometer (Δl_i) and the original gauge length of 200 mm, expressed as a percentage. Furthermore, a paired t-test was conducted for statistical validation. Specifically, force-strain data at the same measurement point under identical loading conditions were analyzed across the two growth stages. The slope of the force–strain curve denotes the sensitivity of local strain response to the applied pulling force. It represents the effective stiffness at the measurement point, which incorporates both material properties and geometric factors contributing to this changes. A significance level of $p < 0.05$ was considered to indicate statistically significant differences between the two stages, whereas $p \geq 0.05$ indicated no significant difference.

For the rotational behavior at the stem base, in addition to comparing the changes in rotation under the same force, the anchorage of roots was also analyzed with reference to (Ennos, 2000; Lundström et al., 2007a) and calculated as Eq. (3).

$$K = \frac{M}{\theta}, \tag{3}$$

where K refers to the anchorage of roots in N·mm/°. The bending moment (M) was derived from FEM in Section 2.4 when applied the same force as tests. The rotation (θ) was from the analysis of pulling results. The comparison data will be presented in the Results section, and measured data are available upon request.

2.4. Numerical analysis by FEM

FEM analysis was conducted to better understand the stress distribution and overall deformation behavior of different tree systems in two growth stages. In experimental testing, only local deformations were

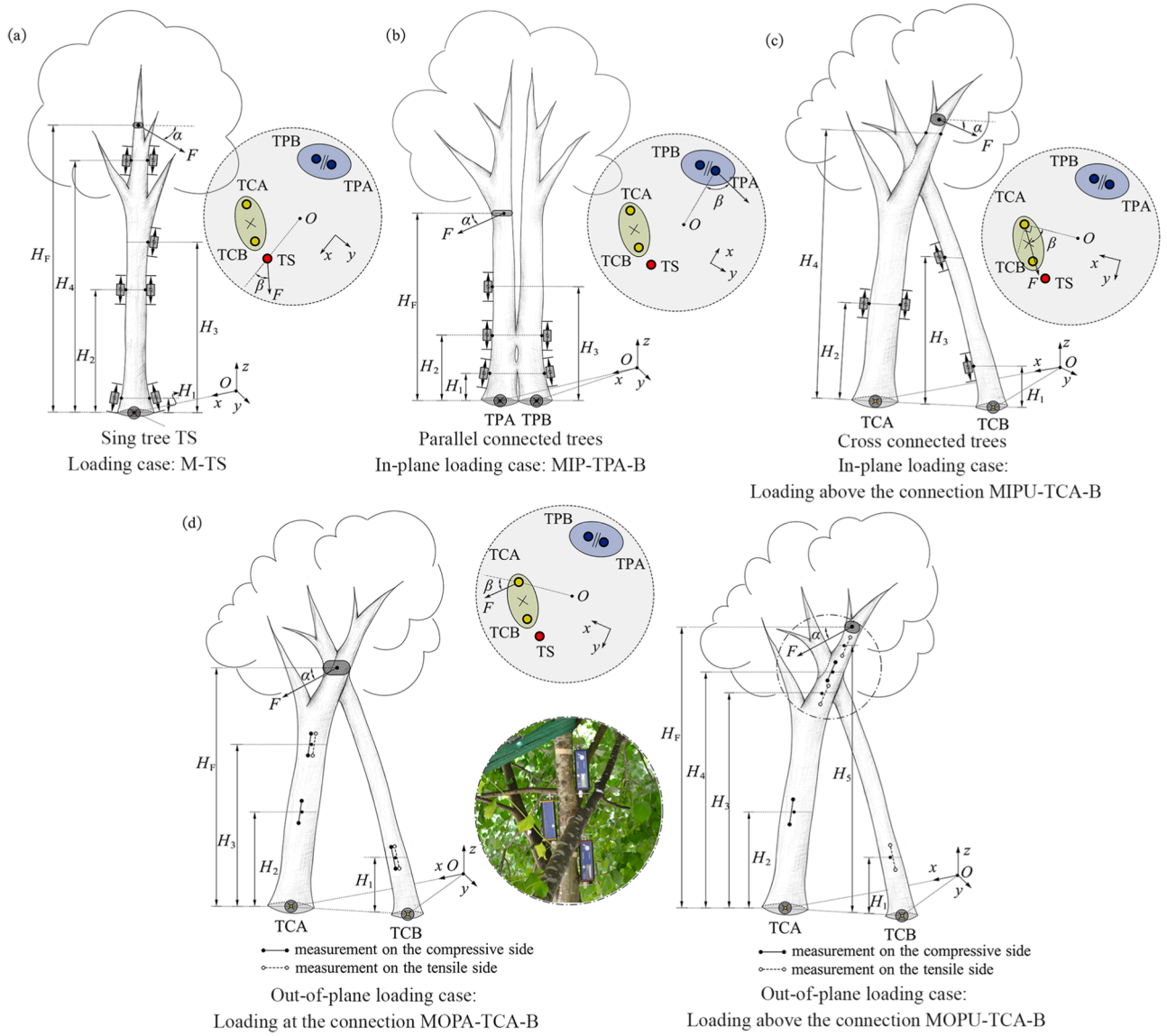

Fig. 6. Schematic diagrams of loading conditions.(a) Loading condition for single tree TS (M-TS); (b) In-plane loading condition for parallel connected trees TPA and TPB (MIP-TPA-B); (c) In-plane loading condition for cross-connected trees TCA and TCB (MIPU-TCA-B); (d) Out-of-plane loading conditions for cross connected trees TCA and TCB, left: loading point at the connection (MOPA-TCA-B), right: loading point above the connection (MOPU-TCA-B). Measurement points are placed on both the tensile and compressive sides. Heights of each measurement position are detailed in Table 2.

Table 2
Groups of pulling tests and their measured points.

Tree description	Loading case ID	Measurement height (m)					Force height (m)	Force angle (degree)	
		H_1	H_2	H_3	H_4	H_5	H_F	α	β
Single tree: TS	M-TS	0.2	1.4	1.9	2.5	–	2.5	12.6	10.0
Parallel connected trees: TPA and TPB	MIP-TPA-B	0.2	0.5	0.8	–	–	1.9	19.2	89.0
Cross connected trees: TCA and TCB	MIPU-TCA-B	0.4	0.8	1.4	–	–	2.5	29.1	65.0
	MOPA-TCA-B	0.4	0.8	1.5	–	–	2.2	10.5	50.0
	MOPU-TCA-B	0.4	0.8	2.0	2.2	2.4	2.5	17.2	50.0

measured, which made it difficult to assess the structural response of the entire system. Furthermore, calculating root bending moments using simplified cantilever beam models (Niklas and Spatz, 1999) overlooks the actual tree morphology and fails to account for canopy weight and second-order geometric effects. To address this, the FEM model incorporated detailed geometric features of the tree stems from the measurements in Section 2.2 (Fig. 4). The applied forces followed the same location and direction as in the pulling tests (Fig. 6). This helped in calculating the basal bending moments, stress distributions, and overall displacement at the loading points in both growth stages.

In modeling stems, the fiber directions at the connection were defined on the basis of the dominant stem axis, typically the stem with the largest diameter (Fig. 7). Previous studies (Wang et al., 2025a, b) indicated the presence of bundles of merged fibers in the interfacial region. Given that this study focused on the elastic range, the fiber orientation was simplified to align with the axis of the dominant tree.

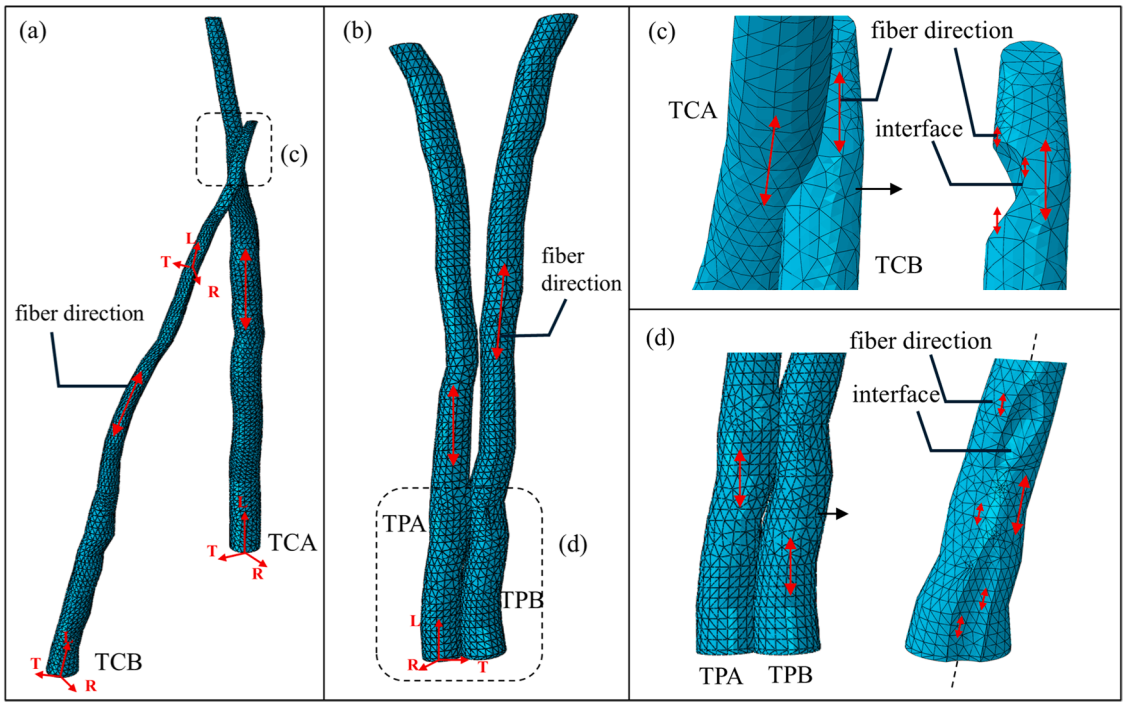

Fig. 7. Finite element modeling based on geometric measurements of tree systems and the indication of fiber directions.(a) FEM model of the cross-connected tree system (TCA–TCB), with the fiber orientation aligned along the longitudinal axis of the central pith; (b) FEM model of the parallel-connected tree system (TPA–TPB); (c) In the cross connected region, the material orientation in the overlapping wood zone is assigned according to the grain direction of the dominant tree (TCA). (d) In the parallel connected region, the material grain direction is assigned along TPA's pith.

For example, as shown in Fig. 7a and c, the tree TCA has a larger diameter at the connection, thus, the orientation of the fiber at the interface was defined along the longitudinal direction of the TCA. Similarly, the definition fiber directions for TPA and TPB can be seen in Fig. 7b and d.

The material properties were not measured directly in this experiment. The density of wood was established at 1000 kg/m^3 from (Šilinskas et al., 2021). The Young's modulus was estimated on the basis of data from the single tree TS. The pulling force measured in the test was input into the finite element model; and strains at 1.4 m was used for validation. A reverse calculation was performed. The Young's modulus was adjusted from 8000 to 10,000 MPa in 100 MPa increments. The best match to the experimental strain was found at 8300 MPa. The weight ratio between stem and canopy was adopted from (Wessolly and Erb, 2016). These parameters are listed in Table 3. As the analysis is based on relative comparisons between two growth stages, it is assumed that the parameter values are identical in both stages. The stem was modeled using homogeneous solid elements of C3D10. The orientation of the material is shown in Fig. 7, with a mesh size of approximately 25 mm. According to EN384 (European Standard, 2022), the ratio of modulus of elasticity between longitudinal and radial directions was established at 15, and the ratio between the longitudinal modulus and shear modulus was established at 16. The canopy was simplified as a point mass located at the top of the stem, with a mass equal to 30 % of the weight of the stem, based on (Wessolly and Erb 2016). The material properties were assumed to remain unchanged during the two-year period, and only geometric changes were modeled. All the calculations were conducted in ABAQUS software. Based on the measured actual coordinates and geometry of trees, as well as the applied canopy weight, both the inclination resulting from growth and the second-order effects induced by self-weight during pulling simulation can be computed.

3. Results

3.1. Growth differences between tree systems

The geometric growth of trees was assessed by analyzing the distribution of the cross-sectional moment of inertia according to Section 2.2. Due to the conical shape of the tree stems, the moment of inertia at the base was consistently greater than that at the DBH. Among the five measured trees, this difference ranged mainly between 2 and 5 times. During two growing seasons, the tree TS showed a relatively uniform increase in moment of inertia from the base to the top, with an overall growth ratio of approximately three times (Fig. 8a and d). In parallel connected trees TPA and TPB, the increase ranged between 2 and 3 times (Fig. 8c and d). For the TCA tree (Fig. 8b), branching occurred at a height of 2 m, and only the diameter of the main stem was measured beyond the point, resulting in a drop in measurement. In the tree TCB (Fig. 8b and e), the stem inclination led to uneven structural growth and lateral branches occurred, therefore it had constantly pruning during the measurements.

Table 3
Parameters for FEM analysis.

Density (g/mm^3)	Canopy to stem weight ratio	Young's modulus (MPa)			Shear modulus (MPa)			Poisson's ratio		
		E_L	E_R	E_T	G_{LR}	G_{LT}	G_{RT}	μ_{RT}	μ_{LR}	μ_{LT}
0.001	0.3	8300	553	553	519	519	51.9	0.4	0.2	0.2

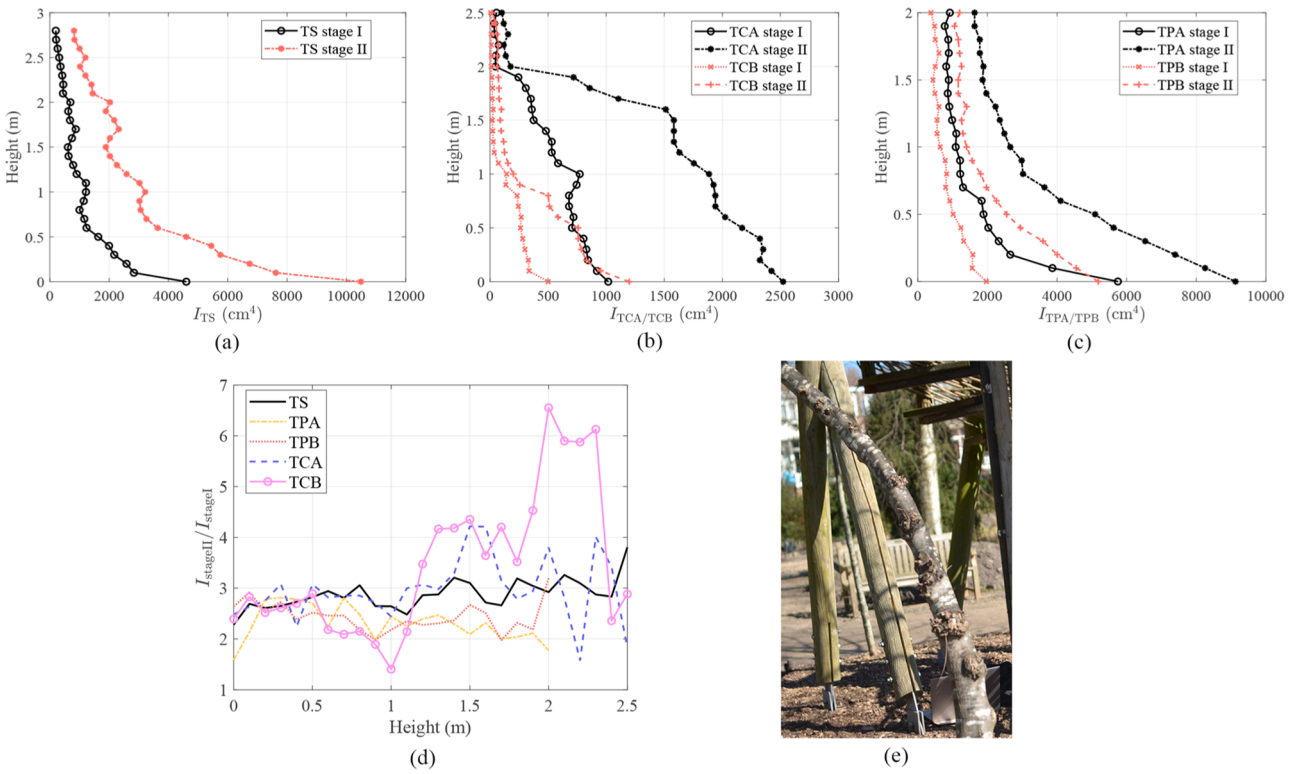

Fig. 8. Changes in cross-sectional moment of inertia between two growth stages (I and II). (a) Moment of inertia distribution in single tree TS; (b) in cross connected trees TCA and TCB; (c) in parallel connected trees TPA and TPB; (d) Variation of the ratio (Stage II / Stage I) along tree height; (e) Knot distributions of tree TCB.

3.2. Assessment of stem performance before and after a two-year growth period

According to the measurements of pulling tests described in Section 2.3, Fig. 9 summarizes the mechanical performance of a single tree, as well as the in-plane performance of connected trees with cross and parallel connections. Each measured point is labeled using the format: "Tree ID and growth stage–measured height–Tension (T)/Compression (C)". For example, "TSI-14-T" refers to the result of the tensile strains at a height of 1.4 m in the TS tree during growth stage I. "TSII-24-C" refers to the result of the compressive strains at a height of 2.4 m in the TS tree during growth stage II.

- Single tree TS, the loading case M-TS

For the single tree TS (Fig. 9a-c), local strains under tension and compression appeared to be approximately symmetrical in both stage I (Fig. 9a) and stage II (Fig. 9b). At a height of 0.2 m on the compression side (TS-2-C), the measured location was close to the root bridge. During loading in stage II, it was observed that the root bridge influenced movement, resulting in greater deformation at this measured location (Fig. 9b). Due to the presence of a knot at 0.8 m, no measurement point could be placed there. Instead, the 1.4 m position was used as an approximate substitute. It can be seen that at this height (TS-14-T) the stain was the largest. As shown in Fig. 9c, when the pulling force was set at 1000 N, and as discussed in (Wessolly and Erb, 2016), the central region within the stem exhibited a more significant deformation. It indicated a higher probability of structural failure in that zone. As shown in Fig. 9c, under the same pulling force, the strain in stage II was 0.52–0.91 times that in stage I at six out of seven measurement points and statistically significant ($p = 0.014 < 0.05$). However, the slopes of the force-strain curves did not differ significant between the two stages ($p = 0.084 > 0.05$).

- Parallel connected trees TPA and TPB, the in-plane loading case MIP-TPA-B

For the parallel connected trees TPA and TPB, the connection is located at a height of 0.5 m. Below this point, when the pulling force was applied to TPA, the compressive strain in TPA at the same height was greater than the tensile strain in TPB. This phenomenon was observed consistently in both measurements (stage I in Fig. 9d, stage II in Fig. 9e). It showed that the connection allowed forces to transfer between the two trees, but tree TPA played a dominant role for load resistance (Fig. 9j). As a result, the external load was partially distributed, which allowed both trees to share mechanical loads and achieve a degree of load mitigation through structural coupling. In this system, it was observed that the measurement point at 0.8 m (TPA-8-C) was the first to reach the failure threshold, indicating a potential weak zone in the structure. Paired comparisons of the force–strain slopes and the strain at the same force level (Fig. 9f) between the two stages showed no statistically significant differences (slope: $p = 0.375 > 0.05$, strain: $p = 0.162 > 0.05$).

- Cross connected trees TCA and TCB, the in-plane loading case MIPU-TCA-B

For the cross connected trees TCA and TCB, under the in-plane pulling scenario MIPU-TCA-B, the force was applied above the cross connection at the height of 2.5 m. Tree TCA has a twice larger DBH than tree TCB. When comparing the local deformation in stage I (Fig. 9g) and stage II (Fig. 9h), several observations can be seen. At 2.4 m in tree TCA (TCA-24-C), significant deformation was observed; and this location was 0.2 m above the cross connection and 0.1 m below the force location. In tree TCB, the maximum strain occurred at a height of 1.4 m (TCB-14-C), while in TCA, the strain below the connection was reduced. Particularly, at 0.8 m of TCA (TCA-8-C), the deformation was significantly reduced. This indicated that the connection provided structural support to tree TCA, which presented a pronounced bracing effect. However, because

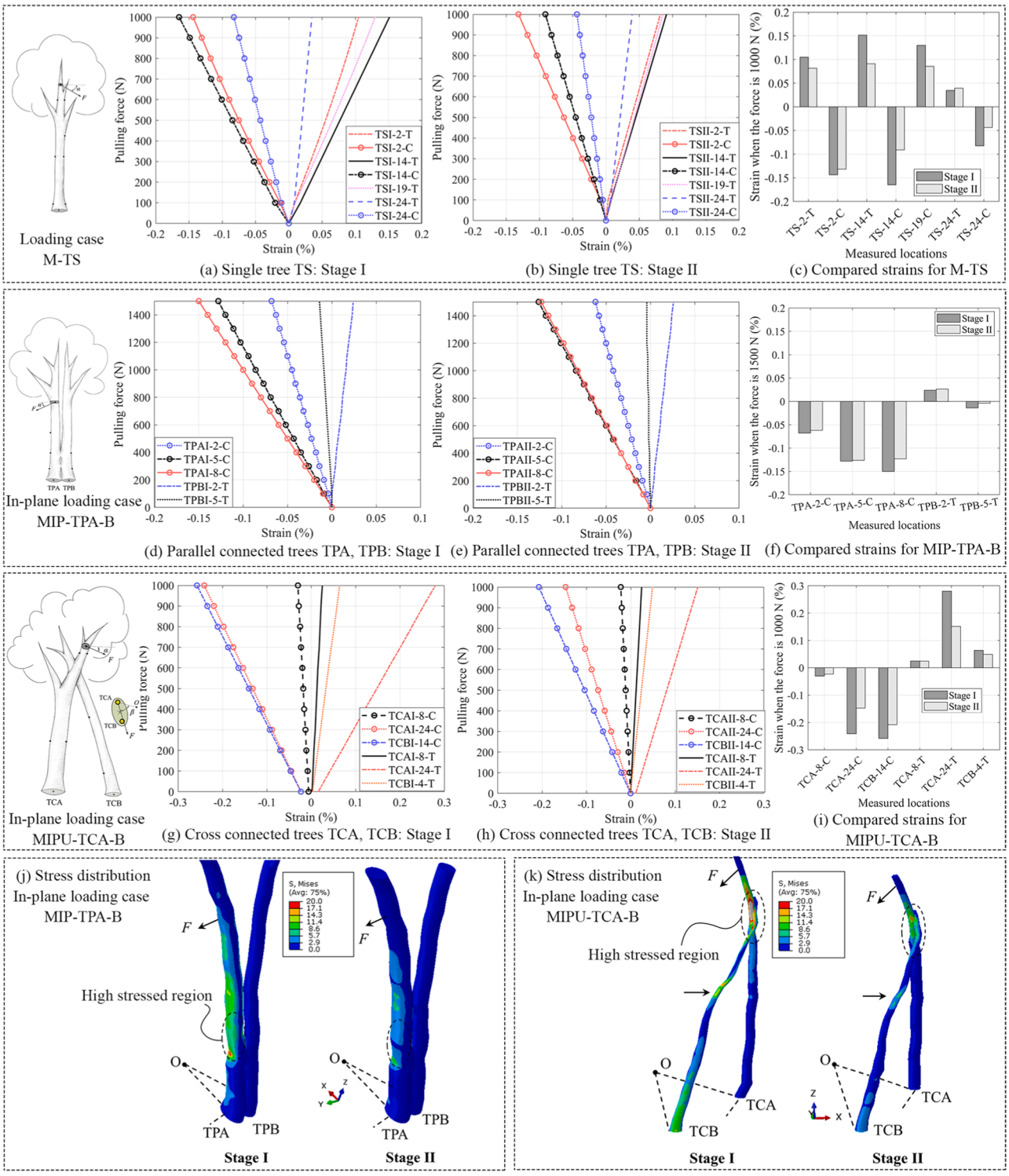

Fig. 9. Mechanical performance of a single tree and the in-plane performance of cross connected trees (TCA and TCB) as well as parallel connected trees (TPA and TPB). For the single tree (TS), the mechanical performance in the loading case M-TS is shown in the panel (a)–(c), including comparisons of force–strain relationships between two growth stages and strain differences under identical force levels. The panel (d)–(f) presents the in-plane responses of parallel connected trees (TPA and TPB) under the loading case MIP-TPA-B. For the cross connected trees (TCA and TCB), the in-plane mechanical responses under loading applied above the connection are shown in panels (g)–(h), which corresponds to the loading case MIPU-TCA-B. (j) illustrates the stress distribution corresponding to MIP-TPA-B, while (k) shows the stress analysis for MIPU-TCA-B. The legend in each panel denotes tree ID stage-measurement height-compression/tension. For instance, TCAI-8-C indicates a measurement taken in stage I on tree TCA at a height of 0.8 m on the compressive side.

the tree TCB has a diameter smaller than TCA, which made TCA the dominant tree within the system. When the pulling force was applied, tree TCB exhibited considerable torsional deformation. Its deformation was much greater than that of the TCA. This suggests that TCB experienced more complex structural responses and carried a higher risk of failure under such loading condition. At the same loading level (Fig. 9i), the strains in stage II were 0.54–0.98 times that in stage I. Although variations in both the slope and the strain were observed between stage I and stage II, these differences did not reach the threshold of statistical significance (slope: $p = 0.053 > 0.05$, strain: $p = 0.069 > 0.05$).

Under the two in-plane tensile loading conditions (Fig. 9d-f and Fig. 9g-i), the stress distributions of the cross connected TCA–TCB and parallel connected TPA–TPB systems are shown in Fig. 9j and k. In terms of cross connected TCA-TCB, as previously observed in experimental measurements, when the loading point was located above the connection, the connection became a region of stress concentration and was prone to failure, as pointed by the dashed circles. Conversely, below the connection, the mechanical response was reduced. In this system, TCB exhibited a torsional response, with a high risk of failure around the 1.4 m height. Despite this, the cross connection had a higher risk of failure. In contrast, the parallel connected TPA–TPB system showed reduced stress below the connection. However, in the upper region above the connection, particularly around the connection itself, bending deformation was more likely to occur, making it a potential structural weak point.

- Cross connected trees, the out-of-plane loading case at the connection MOPA-TCA-B and above the connection MOPU-TCA-B

To better understand this behavior under out-of-plane pulling cases, the mechanical responses of the cross connected tree system under two different loading positions were compared (Fig. 10). In Fig. 10a-c, the force was applied directly at the connection (height 2.2 m), while in Fig. 10d-f, the load was applied higher, at 2.5 m (see Fig. 6 for a detailed setup). In the first case (MOPA-TCA-B), regions at 0.8 m in TCA (TCA-8-C) showed high risk. The tensile and compressive sides presented relatively symmetric. Under this loading condition, the strains in stage II were 0.28–0.83 times that in stage I, and both the strain and the slope were significantly reduced compared with stage I (strain: $p = 0.041 < 0.05$, slope: $p = 0.008 < 0.05$).

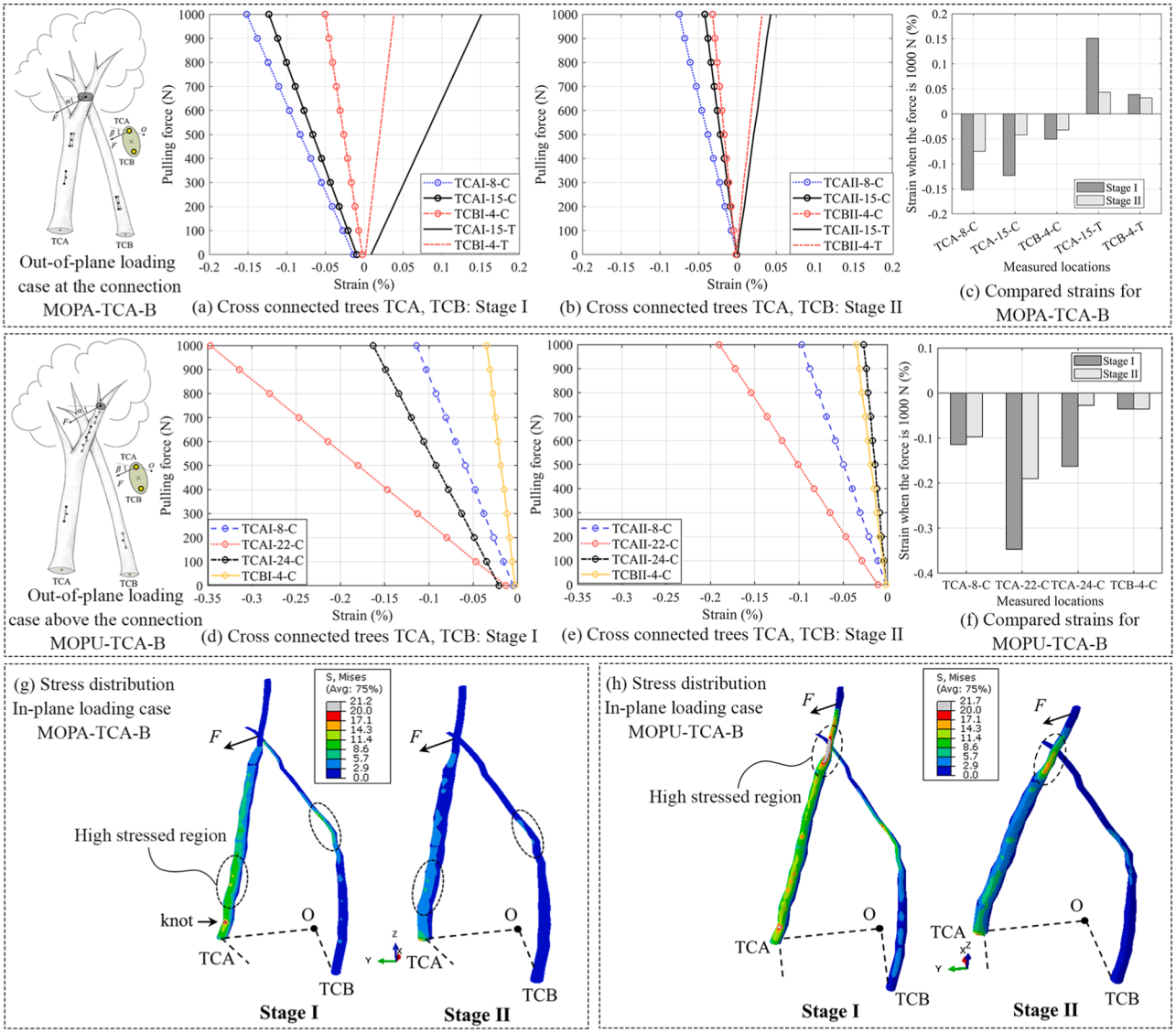

Fig. 10. Mechanical performance of the out-of-plane loading on cross-connected trees (TCA and TCB). When the loading point is located at the connection, the loading case is MOPA-TCA-B (a–c). When the loading point is located 2.5 m above, on top of the connection, the loading case is MOPU-TCA-B (d–f). The corresponding stress distributions for these two loading cases are shown in (g) and (h), respectively.

In the latter case (MOPU-TCA-B), it can be compared with the in-plane loading (MIPU-TCA-B in Fig. 9) as the directions of forces were at the same height and perpendicular to each other. Using the location at 0.8 m in TCA (TCA-8) below the connection as a reference to compare, the in-plane loading case showed a significant reduction in local deformation. This indicated that the connection provided a more effective support in the in-plane in comparison to the out-of-plane loading. Statistically, no significant differences were found in either strain or slope between the two stages under this loading condition (strain: $p = 0.150 > 0.05$, slope: $p = 0.325 > 0.05$).

Based on the stress distribution in Fig. 10 from FEM analysis, when the loading point occurred at the connection (Fig. 10g), the lower stem of the TCA (0.8 m) and the 1.4 m section of TCB were high-risk zones of failure. The location at 1.4 m in TCB was not able to measure during the pulling tests. FEM in this case can help to identify potential weak area. When the loading point was above the connection (Fig. 10h), the stress concentration shifted, and the connection itself showed a higher failure risk, even exceeding that of the 1.4 m section of TCB. This suggested that the connection functioned not only as a load-transmitting element, but also acted as a redundant structural barrier, thereby it helped improve the overall failure resistance of the system.

A comparative analysis of strains and the slopes of the force–strain curves across all measurement points showed that, at the data level, strains were reduced in 25 out of 27 points (92.6 %) in stage II, while the slopes, representing the local effective stiffness, increased in 24 out of 27 points (88.9 %). However, statistical tests indicated that neither difference reached the level of significance (strain: $p = 0.203 > 0.05$, slope: $p = 0.139 > 0.05$).

3.3. *Comparison of rotation behavior at the stem base and the overall deformation in the tree systems*

As described in Section 2.3, the comparison of rotation angle (Fig. 11a) and anchorage stiffness (Fig. 11b) between the two growth stages found that, except for the in-plane pulling condition in the cross connected system, most cases exhibited a decrease in base rotation after the two-year growing period; and the anchorage stiffness (Eq. (3)) increased by a factor of 1 to 2. For single tree TS, the base rotation angle decreased significantly under the same applied force after two-year growth, and the anchorage stiffness approximately doubled, which indicated a structural enhancement. In the parallel connected TPA–TPB system, under in-plane tensile loading, both trees tended to rotate synchronously in the direction of the applied force. However, TPA exhibited greater anchorage stiffness than TPB. It may suggest that TPA played a dominant structural role in this loading condition. In the cross connected TCA–TCB system, under in-plane pulling, the rotation angles of both trees increased during stage II. This may be attributed to the out-of-plane torsion effects induced by the shifted force direction during testing, resulting in additional bending at the base. Despite this, TCB showed a larger increase in anchorage stiffness compared to TCA. Under out-of-plane pulling conditions, both TCA and TCB reinforced their anchorage systems after adaptive growth, with a reduction in the rotational response, which indicated enhanced structural stability.

Compared to the single tree TS, all the connected systems showed smaller deformations, which demonstrated the positive contribution of structural connections to overall stability (Fig. 11c). Among the connected tree systems, the cross connected system exhibited larger deformation under out-of-plane tensile loading. In contrast, under in-plane loading, the deformation was significantly reduced. It was because the connection provided more effective support within the connecting plane. This enhanced performance was attributed to the triangular stability formed by the configuration in the plane, which effectively restricts the deformation. For the parallel connected system, the connection is located near the base of the stems, which also contributed to reducing deformation, particularly in the lower region.

4. Discussion

The results above demonstrate that both growth and self-growing connections improve mechanical performance. Nevertheless, several limitations in the experimental method, modeling assumptions, and interpretation of results need further discussion.

- Limitations and improvements of the experimental method

In this study, the unidirectional pulling test was used to simulate wind loads, which is a simplified method commonly used under field conditions (Peltola et al., 2000; Detter et al., 2023; Seipulis et al., 2024). However, it does not fully represent the complex combination of bending, shear, and torsional loads exerted by natural wind (de Langre, 2008). While this method offers advantages in operability and repeatability, its limitation lies in the inability to accurately control and measure deformations, as well as to capture multi-dimensional loading responses. Sample selection was also restricted in this study. The formation of self-growing connections requires long cultivation period (approximately taking two years to form firmly), and tree specimens are relatively large and few in number. Therefore, the study relied on stage-based comparisons over the course of growth. In the analysis, the elastic modulus of wood was assumed to remain constant during growth; however, previous studies have shown that the modulus varies with growth ring structure, tree age, height, etc. (Huang et al., 2024; Mańkowski et al., 2025), which should be incorporated in future studies using measured material data.

Regarding measurements, strain sensors were applied only locally,

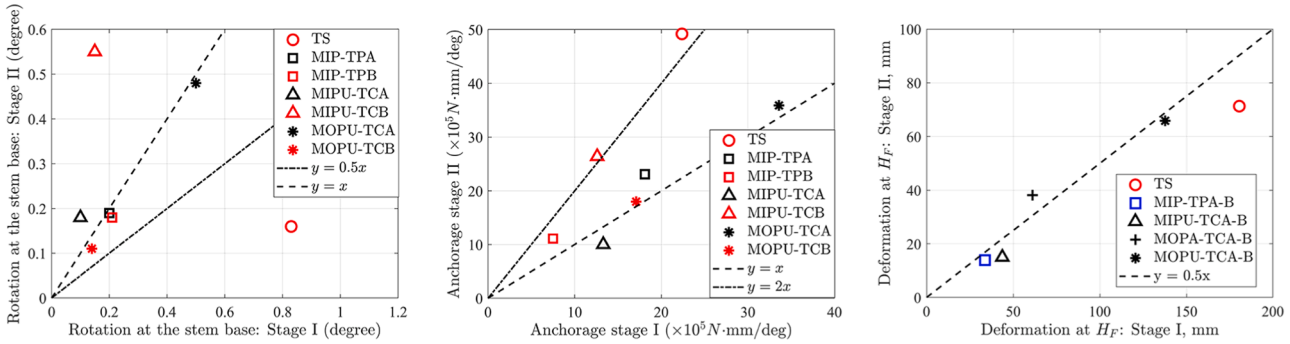

Fig. 11. Rotational behavior at the stem base and the overall deformation in the tree systems in stage I and stage II. In the legend, TS denotes the single tree. For the parallel connected trees under in-plane loading, trees include MIP-TPA and MIP-TPB. For the cross connected trees under out-of-plane loading, trees include MOPU-TCA and MOPU-TCB. For the cross connected trees under in-plane loading, trees include MIPU-TCA and MIPU-TCB.

and full-field strain could not be captured. Displacement measurements at the loading point were also incomplete due to field limitations. Future improvements could involve 3D point cloud scanning for capturing detailed tree geometry (Jackson et al. 2019b) and the use of digital image correlation (Dahle, 2017; Tippner et al., 2019) to obtain multi-point, full-field strain and displacement data, thereby improving both accuracy and representativeness.

In finite element modeling, the material properties were assumed to be uniform and constant with growth, representing a simplified analysis. At the connection, the fiber orientation was approximated according to the dominant stem, while ignoring local variations. Nevertheless, previous studies have shown that fiber distribution at the interface can be highly complex, involving intertwined and asymmetric patterns (Wang et al., 2025a). Similar simplifications of fiber structures have also been made in studies of nature tree connections considering the high variability of the growth (Slater et al., 2014; Middleton et al., 2023). Accurately determining fiber orientation and distribution in naturally fused connections remains an important subject for future detailed investigations, particularly for improving the reliability of numerical analyses.

- Effects of diameter growth on rigidity and deformation

Radial growth substantially contributes the mechanical response. For the single tree (TS), the DBH increased by 32 % between stage I and stage II. Simplified cantilever beam theory (Niklas and Spatz, 1999) predicts that the moment of inertia would increase about threefold, maximum bending strain would decrease by approximately 56 %, and free-end deflection would reduce by around 67 %. Experimental results showed comparable trends for the TS tree: the moment of inertia increased by 2.4–3.9 times (Fig. 8), local strain decreased by 8–48 % (Fig. 9), and free-end displacement was reduced by around 60 % (Fig. 11). While the experimental and theoretical results were broadly consistent, discrepancies can be attributed to the tapered geometry of tree stems, rather than uniform cylinders, and the spatial variation in material properties along the height and across growth rings, making homogeneous beam assumptions insufficient to fully capture the anisotropy of real stems.

- Statistical significance versus observed trends

As presented in Section 3.2, local strain comparisons showed that stage II generally exhibited reduced strain and increased curve slopes compared with stage I. However, statistical analyses did not yield significant differences. Several factors may explain this discrepancy. First, the sample size was limited: only 4–6 measuring points per loading case and 27 in total, so even a few outliers could strongly affect the overall significance. For instance, at 0.2 m height in the single tree TS, the formation of a root bridge introduced local rotation, causing deviation from the general trend. Second, the magnitudes of local deformation at some points (e.g., TPB-5, TCA-8) were relatively small, making subtle differences difficult to detect within the resolution limits of the sensors. Third, biological variability in growth and wood properties introduces inherent randomness, meaning that even under similar conditions, local responses may deviate from the overall pattern. Therefore, although statistical significance was not achieved, the observed trends remain informative. Increasing sample size, measurement points, and instrument precision in future studies would allow clearer identification of growth effects on local mechanical responses.

- Long-term observations and implications for structural design

The cross and parallel connection methods validated in this study demonstrated the potential to improve lateral load-bearing capacity. From a structural mechanics perspective, cross connections form triangular stable units that significantly increase rigidity, while parallel connections enlarge the effective load-bearing area and improve redundancy. In this study, the parallel connection located at the lower part of the stems (at a height of 0.5 m) enlarged the load transfer area near the base. This allowed loads to be distributed before reaching the tree base, enabling both stems to share the load and significantly reducing basal rotation. Under in-plane loading, the cross connected pattern formed triangular supports that effectively reduced displacement. Under out-of-plane loading, the stiffness was lower; however, cooperative movement between stems still helped to reduce deformation to some extent. These results demonstrate the effectiveness of the cross connection in enhancing overall lateral resistance.

Although only two typical configurations were examined, the design potential is much broader. Parameters such as crossing angle and connection height may also influence performance. Moreover, tree species with natural grafting abilities, such as willow, poplar, and weeping fig (Wang et al., 2020, 2025a), provide opportunities for diverse structural strategies. Future studies may explore different species, crossing geometries, and growth stages to compare structural responses under varying conditions. Long-term monitoring combined with multi-scale numerical modeling will be essential to further understand the adaptive and stabilizing roles of such bio-architectural systems in natural environments.

5. Conclusions

In this study, naturally fused self-growing connections were used to connect two trees, resulting in the formation of two types of systems: cross connected and parallel connected tree systems. They were compared with a single tree to assess the mechanical performance. Due to the different connecting strategies, each tree system exhibited different structural responses under directional loading. Through a combination of pulling testing and FEM analysis, and using a two-year growing period as the comparative basis, the key findings are as follows:

1) After a two-year growing period, the interconnected tree systems exhibited a trend of increased stiffness, reduced local strain, decreased basal rotation, improved root anchorage, and lower overall deformation under identical loading conditions. However, these improvements did not reach strong statistical significance, which may be attributed to the limited sample size, inherent variability in tree growth, and the precision limits of field measurements.
2) Compared to a single tree, the presence of connections improved the stiffness of interconnected tree systems, thus reducing responses to deformation under lateral forces. This effect is more pronounced under loading conditions in the connected plane.
3) In the parallel connected system, the connection located near the base of the stem contributed to the redistribution of forces in the lower region, which led to improved stability in the root zone.
4) In the cross connected system, the connection enabled load sharing between the two trees. It created a redundant load path that improved the system's resistance to failure. Compared to out-of-plane loading, in-plane loading had a stronger bracing effect, as evidenced by smaller deformations. The cross connection acted as a stabilizing path and formed a triangular load-bearing structure.

These findings demonstrate that both connection strategies enhance the structural resilience of tree systems. The cross and parallel connection configurations can be seen as fundamental bio-structural units. It can offer important insights for the design of self-growing structures and biomimetic architectural systems.

In future research, refined measurements of tree geometry could be combined with spatial characterization of wood material properties, as well as high-resolution control measurements using digital image correlation, to enhance the accuracy of experimental data. On the design side, varying connection strategies could be systematically explored, including different species, connecting heights, crossing angles,

diameter ratios, growth stages, etc. Expanding the number of experimental specimens will also be crucial for improving statistical robustness and for further validating both the structural performance and ecological benefits of interconnected tree systems.

CRediT authorship contribution statement

Xiuli Wang: Writing – original draft, Visualization, Validation, Methodology, Investigation, Formal analysis, Data curation, Conceptualization. **Wolfgang Gard:** Writing – review & editing, Supervision, Project administration, Conceptualization. **Abhijith Kamath:** Writing – review & editing, Visualization, Investigation. **Jan-Willem van de Kuilen:** Writing – review & editing, Supervision, Resources, Project administration, Funding acquisition, Conceptualization.

Declaration of competing interest

The authors declare that they have no known competing financial interests or personal relationships that could have appeared to influence the work reported in this paper.

Acknowledgements

The support of Bob Ursem, James Byng, Eveline Oranje, Anne Nuijten, Tessa Lievestro and Dennis de Goederen during the research is greatly appreciated.

Data availability

Data will be made available on request.

References

Alméras, T., Fournier, M., 2009. Biomechanical design and long-term stability of trees: morphological and wood traits involved in the balance between weight increase and the gravitropic reaction. J. Theor. Biol. 256, 370–381. https://doi.org/10.1016/j.jtbi.2008.10.011.

Cucchi, V., Meredieu, C., Stokes, A., et al., 2005. Modelling the windthrow risk for simulated forest stands of Maritime pine (*Pinus pinaster* Ait.). For. Ecol. Manage 213, 184–196. https://doi.org/10.1016/J.FORECO.2005.03.019.

Dahle, G., 2017. Influence of bark on the mapping of mechanical strain using digital image correlation. Wood. Sci. Technol. 51, 1469–1477. https://doi.org/10.1007/s00226-017-0947-0.

Dahle, G., James, K., Kane, B., et al., 2017. A review of factors that affect the static load-bearing capacity of urban trees. Arboric Urban For 43, 89–106. https://doi.org/10.48044/jauf.2017.009.

de Langre, E., 2008. Effects of wind on plants. Annu Rev. Fluid. Mech. 40, 141–168. https://doi.org/10.1146/annurev.fluid.40.111406.102135.

Detter, A., Rust, S., Krišāns, O., 2023. Experimental test of non-destructive methods to assess the anchorage of trees. Forests 14, 1–18. https://doi.org/10.3390/f14030533.

Dlouhá, J., Défossez, P., Dongmo, Keumo, Jiazet, J.H., et al., 2024. Mechanical vulnerability of beech (*Fagus sylvatica* L.) poles after thinning: securing stem or roots is risk dependent. For. Ecol. Manage. 552, 121523. https://doi.org/10.1016/j.foreco.2023.121523.

Dlouhá, J., Moulia, B., Fournier, M., et al., 2025. Beyond the perception of wind only as a meteorological hazard: importance of mechanobiology for biomass allocation, forest ecology and management. Ann. For. Sci. 82, 1–11. https://doi.org/10.1186/S13595-024-01271-6.

Dupuy, L., Fourcaud, T., Stokes, A., 2005. A numerical investigation into factors affecting the anchorage of roots in tension. Eur. J. Soil. Sci. 56, 319–327. https://doi.org/10.1111/J.1365-2389.2004.00666.X.

Ennos, A., 2000. The mechanics of root anchorage. Adv. Bot. Res. 33, 133–157. https://doi.org/10.1016/S0065-2296(00)33042-7.

European Standard (2022) EN 384: Structural Timber - Determination of characteristic values of mechanical properties and density.

Fourcaud, T., Ji, J.N., Zhang, Z.Q., Stokes, A., 2008. Understanding the impact of root morphology on overturning mechanisms: a modelling approach. Ann. Bot. 101, 1267–1280. https://doi.org/10.1093/aob/mcm245.

Gardiner, B.A., Berry, P., Moulia, B., 2016. Review: wind impacts on plant growth, mechanics and damage. Plant Sci. 245, 94–118. https://doi.org/10.1016/j.plantsci.2016.01.006.

Gardiner, B.A., Quine, C.P., 2000. Management of forests to reduce the risk of abiotic damage - A review with particular reference to the effects of strong winds. For. Ecol. Manage. 135, 261–277. https://doi.org/10.1016/S0378-1127(00)00285-1.

Goldschmidt, E.E., 2014. Plant grafting: new mechanisms, evolutionary implications. Front. Plant Sci. 5, 109919. https://doi.org/10.3389/FPLS.2014.00727.

Hamant, O., Moulia, B., 2016. How do plants read their own shapes? New. Phytol. 212, 333–337. https://doi.org/10.1111/NPH.14143.

Huang, H., Li, Z., Li, Y., et al., 2024. Comparative studies on tensile mechanical properties of water-saturated earlywood and latewood within the same growth ring from Masson pine. Forests 15, 589. https://doi.org/10.3390/f15040589.

Jackson, T., Shenkin, A., Moore, J., et al., 2019a. An architectural understanding of natural sway frequencies in trees. J. R. Soc. Interface 16. https://doi.org/10.1098/RSIF.2019.0116.

Jackson, T., Shenkin, A., Wellpott, A., et al., 2019b. Finite element analysis of trees in the wind based on terrestrial laser scanning data. Agric. For. Meteorol. 265, 137–144. https://doi.org/10.1016/J.AGRFORMET.2018.11.014.

Kragler, F., Bock, R., 2025. The biology of grafting and its applications in studying information exchange between plants. Nat. Plants. 11, 955–966. https://doi.org/10.1038/s41477-025-01982-2.

Lievestro T. (2020) Living trees as structural elements for vertical forest engineering. Delft University of Technology. Master thesis.

Ludwig, F., Schwertfreger, H., Storz, O., 2012. Living systems: designing growth in Baubotanik. Archit. Des. 82, 82–87. https://doi.org/10.1002/ad.1383.

Lundström, T., Jonas, T., Stöckli, V., Ammann, W., 2007a. Anchorage of mature conifers: resistive turning moment, root–soil plate geometry and root growth orientation. Tree Physiol. 27, 1217–1227. https://doi.org/10.1093/TREEPHYS/27.9.1217.

Lundström, T., Jonsson, M.J., Kalberer, M., 2007b. The root-soil system of Norway spruce subjected to turning moment: resistance as a function of rotation. Plant Soil. 300, 35–49. https://doi.org/10.1007/S11104-007-9386-2/FIGURES/8.

Mańkowski, P., Karwat, Z., Laskowska, A., 2025. Assessment of the modulus of rupture and modulus of elasticity in static bending of yellow pine earlywood and latewood. Forests 16, 265. https://doi.org/10.3390/f16020265.

Melnyk, C.W., 2017. Plant grafting: insights into tissue regeneration. Regeneration 4, 3–14. https://doi.org/10.1002/REG2.71.

Middleton, W., Erdal, H.I., Detter, A., et al., 2023. Comparing structural models of linear elastic responses to bending in inosculated joints. Trees - Struct. Funct. 37, 891–903. https://doi.org/10.1007/s00468-023-02392-7.

Moulia, B., Coutand, C., Julien, J.L., 2015. Mechanosensitive control of plant growth: bearing the load, sensing, transducing, and responding. Front. Plant Sci. 6, 52. https://doi.org/10.3389/FPLS.2015.00052.

Nicoll, B.C., Gardiner, B.A., Rayner, B., Peace, A.J., 2006. Anchorage of coniferous trees in relation to species, soil type, and rooting depth. Can J. For Res. 36, 1871–1883. https://doi.org/10.1139/X06-072.

Niklas, K.J., Spatz, H.C., 1999. Methods for calculating factors of safety for plant stems. J. Exp. Biol. 202, 3273–3280. https://doi.org/10.1242/JEB.202.23.3273.

Nuijten A.D.W. (2011) Living tree buildings - A research into the possibilities and load bearing capacity of living tree structures. Delft University of Technology. Master thesis.

Peltola, H., 2006. Mechanical stability of trees under static loads. Am. J. Bot. 93, 1501–1511. https://doi.org/10.3732/AJB.93.10.1501.

Peltola, H., Kellomäki, S., Hassinen, A., Granander, M., 2000. Mechanical stability of Scots pine, Norway spruce and birch: an analysis of tree-pulling experiments in Finland. For. Ecol. Manage. 135, 143–153. https://doi.org/10.1016/S0378-1127(00)00306-6.

Seipulis, A., Gardiner, B., Peltola, H., et al., 2024. Geographic variation in resistance of Scots pine (*Pinus sylvestris* L.) to wind loading across different wind environments in Europe. For. Ecol. Manage. 571, 122237. https://doi.org/10.1016/J.FORECO.2024.122237.

Sellier, D., Fourcaud, T., 2009. Crown structure and wood properties: influence on tree sway and response to high winds. Am. J. Bot. 96, 885–896. https://doi.org/10.3732/AJB.0800226.

Sellier, D., Fourcaud, T., Lac, P., 2006. A finite element model for investigating effects of aerial architecture on tree oscillations. Tree Physiol. 26, 799–806. https://doi.org/10.1093/TREEPHYS/26.6.799.

Slater, D., Bradley, R.S., Withers, P.J., Roland Ennos, A., 2014. The anatomy and grain pattern in forks of hazel (*Corylus avellana* L.) and other tree species. Trees - Struct. Funct. 28, 1437–1448. https://doi.org/10.1007/S00468-014-1047-5.

Stokes, A., Salin, F., Kokutse, A.D., et al., 2005. Mechanical resistance of different tree species to rockfall in the French Alps. Plant Soil 107–117. https://doi.org/10.1007/s11104-005-3899-3.

Šilinskas, B., Povilaitienė, A., Urbaitis, G., et al., 2021. The wood quality of small-leaved lime (*Tilia cordata* Mill.) trees in an urban area: a pilot study. Forests 12, 420. https://doi.org/10.3390/F12040420.

Tarroux, E., DesRochers, A., Krause, C., 2010. Effect of natural root grafting on growth response of jack pine (*Pinus banksiana*) after commercial thinning. For. Ecol. Manage 260, 526–535. https://doi.org/10.1016/J.FORECO.2010.05.008.

Telewski, F.W., 2012. Is windswept tree growth negative thigmotropism? Plant Sci. 184, 20–28. https://doi.org/10.1016/J.PLANTSCI.2011.12.001.

Tippner, J., Praus, L., Brabec, M., et al., 2019. Using 3D digital image correlation in an identification of defects of trees subjected to bending. Urban. For. Urban. Green. 46, 126513. https://doi.org/10.1016/j.ufug.2019.126513.

Vovides, A.G., Wimmler, M.C., Schrewe, F., et al., 2021. Cooperative root graft networks benefit mangrove trees under stress. Commun. Biol. 4, 1–8. https://doi.org/10.1038/s42003-021-02044-x.

Wang, X., Gard, W., Borska, H., et al., 2020. Vertical greenery systems: from plants to trees with self-growing interconnections. Eur. J. Wood Wood Prod. 78, 1031–1043. https://doi.org/10.1007/s00107-020-01583-0.

Wang, X., Gard, W., Mosleh, Y., van de Kuilen, J.W.G., 2025a. Morphological analysis of inosculated connections in weeping figs: insights on density, geometry, fiber

structures, and compositional variations. Wood. Sci. Technol. 59, 1–21. https://doi.org/10.1007/S00226-024-01622-6.

Wang, X., Gard, W., van de Kuilen, J.W.G., 2025b. Biomechanical analysis of inosculations (self-growing connections) in *Ficus benjamina* L.: impact of developmental growth levels on mechanical properties. Constr. Build. Mater. 462, 139672. https://doi.org/10.1016/j.conbuildmat.2024.139672.

Wessolly, L., Erb, M., 2016. Manual of Tree Statics and Tree Inspection. Patzer Verlag, Berlin-Hanover.